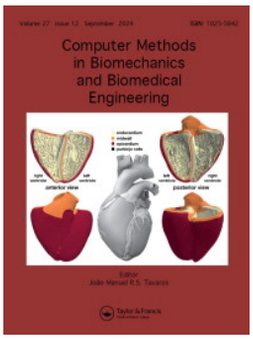

Taylor & Francis
Taylor & Francis Group

Computer Methods in Biomechanics and Biomedical Engineering

ISSN: (Print) (Online) Journal homepage: www.tandfonline.com/journals/gcmb20

Comment on permeability conditions in finite element simulation of bone fracture healing

Agnieszka Sabik

To cite this article: Agnieszka Sabik (14 Sep 2024): Comment on permeability conditions in finite element simulation of bone fracture healing, Computer Methods in Biomechanics and Biomedical Engineering, DOI: 10.1080/10255842.2024.2402878

To link to this article: https://doi.org/10.1080/10255842.2024.2402878

Published online: 14 Sep 2024.

COMPUTER METHODS IN BIOMECHANICS AND BIOMEDICAL ENGINEERING
https://doi.org/10.1080/10255842.2024.2402878

Comment on permeability conditions in finite element simulation of bone fracture healing

Agnieszka Sabik

Department of Mechanics of Materials and Structures, Faculty of Civil and Environmental Engineering, Gdańsk University of Technology, Gdańsk, Poland

ABSTRACT

The most popular model of the bone healing considers the fracture callus as poroelastic medium. As such it requires an assumption of the callus' external permeability. In this work a systematic study of the influence of the permeability of the callus boundary on the simulated bone healing progress is performed. The results show, that these conditions starts to play significant role with the decrease of the callus size. Typically enforced impermeability inhibits the progress of healing during simulation. A remedy for this effect is imposing drainage conditions at the callus' boundary.

ARTICLE HISTORY
Received 14 May 2024
Accepted 2 September 2024

KEYWORDS
Mechano-regulation; secondary healing; poroelastic material; permeability

1. Introduction

Depending on the stabilization techniques, the fusion of the bone fracture can proceed in two ways, i.e. as primary (direct) or secondary (indirect) healing with callus formation (Isaksson et al. 2006; Claes 2011; Augat et al. 2014; Augat et al. 2021). Although both processes possess characteristic disadvantages, and the fracture callus was perceived even as pathological (Augat et al. 2021), nowadays secondary healing is considered as much more biological (Augat et al. 2021) and faster (Foster et al. 2021). This fracture repair takes place in typical stages during which the fracture site changes sequentially from hematoma through soft callus to hard callus. The process is followed by bone remodeling (Quinn et al. 2022a).

Bone healing is a very complex process. Since the experimental revision of this phenomenon is limited, the numerical simulations serve as a good alternative for the evaluation of various stabilization techniques of the fracture site, see e.g. (Miramini et al. 2015; Beirami et al. 2021; Feng et al. 2021; Nayak et al. 2024).

The process depends on many issues, like e.g. specific biological factors or medical treatment. Evidently, the mechanical environment at the fracture site is also very important. For example, indirect healing requires an appropriate amount of movability of the fracture to provide the callus formation (Claes 2011; Augat et al. 2021). In fact, the healing process consists in sequential changes of mesenchymal stem cells (MSC) infiltrating the callus to specific phenotypes, like fibroblasts, chondrocytes or osteoblasts (Lacroix et al. 2002). This tissue differentiation is strongly dependent on mechanical factors. Over the years several mechano-regulation theories were proposed (Isaksson et al. 2006). These theories consider specific mechanical factors as a stimulus of cell differentiation. Pauwels hypothesized, that hydrostatic pressure promotes cartilage formation whereas tensile deviatoric stress is responsible for fibrous tissue arise (Lacroix et al. 2002; Isaksson et al. 2006; Boccaccio et al. 2011). The osteoblast can develop only in zones stabilized by soft callus. On the other hand, in Perren's theory tissue differentiation is driven by strain. Each tissue phenotype cannot form, if the tissue exists in a strain field greater than strain value causing its rupture (Perren 1979; Boccaccio et al. 2011; Claes 2011). This theory is usually called 'interfragmentary strain theory (IFS)' (Isaksson et al. 2006; Augat et al. 2021). The hypothesis of Perren is very simple and intuitive and therefore it is readily used in the evaluation of fixators (Miramini et al. 2016; Augat et al. 2021). Nonetheless, the most popular mechano-regulation theory used in the simulations of the healing process is the proposal of Prendergast

CONTACT Sabik Agnieszka agsa@pg.edu.pl

(Prendergast et al. 1997; Lacroix and Prendergast 2002; Lacroix et al. 2002; Boccaccio et al. 2011; Ma et al. 2018; Mehboob et al. 2020; Mehboob et al. 2024). According to this concept the mechanical stimuli which govern the tissues' differentiation are the octahedral shear strain and velocity of the interstitial fluid. In the opposite to the previous hypotheses this one considers the callus as a biphasic medium. Thus, in this case one of the assumption that must be made in the simulation is the permeability of the callus external boundary. This is mostly assumed to be impermeable (Lacroix et al. 2002; Epari et al. 2006; Isaksson et al. 2006; Ma et al. 2018; Mehboob et al. 2024). The aim of this paper it to review the consequences of this hypothesis. In order to achieve this goal, the series of simulations of axially compressed bone healing is performed with varying drainage conditions of the callus' boundary. The attention is paid to the influence of the callus external permeability on the effect of the simulations. As the importance of these conditions is supposed to increase with the decrease of the callus dimensions, two sizes of the callus are examined. To the best of the author's knowledge such study is original one.

2. Materials and methods

2.1. Bone healing model

The simulation of the bone reconstruction is performed by making use of the model proposed by Lacroix et al. (2002). Figure 1 depicts the scheme of the analysis together with the geometry and loading conditions of the considered models. It must be noticed, that the geometry of the large callus and load scheme are taken after (Lacroix et al. 2002).

In the model with the small callus only the callus size is modified. The callus is assumed to be filled with the granulation tissue at the beginning of the simulation (Lacroix et al. 2002). The healing, in the sense of the simulation, is an iterative process in which the MSC cells' migration is treated as a diffusion phenomenon

$$\frac{\partial c}{\partial t} = D\nabla^2 c \tag{1}$$

In Equation (1) c stands for the normalized cell concentration ($0 \leq c \leq 1$) and D indicates the diffusion coefficient. The value of D is determined basing on the assumption that it provides the steady state concentration ($c = 1$) after 16 weeks in the entire callus (Lacroix et al. 2002; Isaksson et al. 2006; Ma et al. 2018). It is assumed, that the cells flow from the periosteum, surrounding tissues and marrow (Figure 1). The normalized cell concentration at the mentioned boundaries is assumed to be constant ($c = 1$), (Lacroix et al. 2002).

The fracture site is mechanically stimulated by an average load in each day (each iteration). For long bones, like e.g. tibia, usually axial compression is considered with 1 Hz frequency (Lacroix et al. 2002; Isaksson et al. 2006). In the present study the average

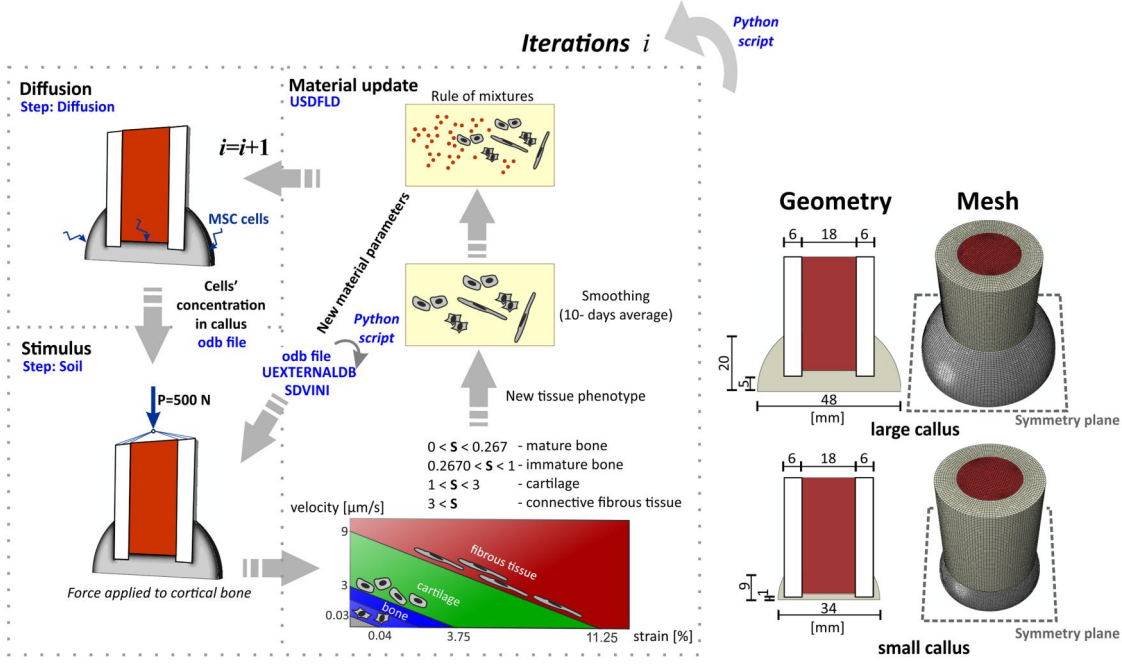

Figure 1. Scheme of the iteration process, geometry data and mesh of the large and small callus.

force is set to 500 N (Lacroix et al. 2002), see Figure 1.

According to the Prendergast theory (Huiskes et al. 1997) the biomechanical stimulus (S) at the peak load is identified by Equation (2)

$$S = \frac{\gamma}{a} + \frac{v}{b} \tag{2}$$

where γ is the octahedral shear strain and v is the interstitial fluid velocity, and $a = 0.0375$ and $b = 3\,\mu m/s$ are the material constants identified experimentally (Huiskes et al. 1997; Prendergast et al. 1997). The stimulus S arising in Equation (2) is assumed to govern the transformation of MSC cells to specific tissue phenotypes, according to: $0 < S < 0.267$ – mature bone, $0.2670 < S < 1$ – immature bone, $1 < S < 3$ – cartilage, $3 < S$ – connective fibrous tissue. Similarly as in Miramini et al. (2016), if $S > 6$, no cell transformation is identified. To prevent the numerical computations from instabilities caused by rapid modifications of material properties, some smoothing strategy must be introduced (Lacroix et al. 2002). In this work it is assumed, that the actual value of the material parameter is a 10 d average P_i, see (Isaksson et al. 2006; Mehboob and Chang 2018; Mehboob and Chang 2019):

$$P_i = \frac{1}{10}\sum_{k=i-9}^{i} P_k \tag{3}$$

where P indicates the material parameter (Young modulus, Poisson ratio, permeability). Table 1 includes the material data adopted in the analysis, that are taken after (Lacroix et al. 2002; Isaksson et al. 2006). Taking into account the concentration of the MSC cells, see Equation (1), the final value of each material parameter is obtained (Lacroix et al. 2002):

$$P_i^{act} = c \cdot P_i + (1 - c) \cdot P_{gran} \tag{4}$$

where P_{gran} is the parameter of the initial granulation tissue.

Table 1. Properties of poroelastic materials (E – young modulus, v – poisson ratio, k-permeability, n-porosity).

Tissue	E [MPa]	v [–]	k [m^4/N·s]	n [–]
Cortical bone	20,000	0.3	10^{-17}	0.04
Marrow	2	0.167	10^{-14}	0.8
Granulation tissue	1	0.167	10^{-14}	0.8
Fibrous connective tissue	2	0.167	10^{-14}	0.8
Cartilage	10	0.167	$5{\cdot}10^{-15}$	0.8
Immature bone	1000	0.3	10^{-13}	0.8
Mature bone	6000	0.3	$3.7{\cdot}10^{-13}$	0.8

2.2. Finite element model

The simulations are performed with the use of the Abaqus (2021) HF12 (Dassault Systemes Simulia Corp.) program. The usage of this software is very popular in the field of biomechanics and mechanobiology since years see, e.g. (Isaksson et al. 2009; Byrne et al. 2011; Merdji et al. 2020; Taharou et al. 2021; Mehboob et al. 2024). The material of the tissues is treated as a fully saturated poroelastic medium. A user subroutines USDFLD, UEXTERNALDB, SDVINI and Python scripts are employed to update the material properties and to transfer the data between the iterations, see Figure 1. In the MSC cells diffusion simulation C3D8PT elements, whereas in the mechanical stimulus analysis (consolidation) the C3D8P elements are adopted. The numbers of elements used in the discretization of each part of the model are collected in Table 2. The approximate size element used in the discretization of the bone, marrow and large callus is 0.6 mm. In modeling of small callus finer mesh (0.4 mm) is adopted to capture the deformability of the thin gap. Increasing the number of elements does not influence the solution.

As the axial load is considered only, one half of the callus is modelled taking advantage of the symmetry conditions relative to the plane perpendicular to the longitudinal axis of the bone, Figure 1.

Typically, in many studies, see e.g. (Lacroix et al. 2002; Epari et al. 2006; Isaksson et al. 2006; Miramini et al. 2015), the external boundaries of all tissues are impermeable. However, in this work full impermeability is imposed only at the bone external boundary, whereas at the callus' external surface various types of permeability conditions are assumed: impermeable, fully permeable (zero pore pressure imposed on the surface) and intermediate. They were achieved by assuming a normal pore fluid flow from the interior of the callus. The flow is determined by the seepage coefficient (k_s). Three levels of seepage coefficient value are considered: large, medium and small, respectively. According to (Abaqus 2021, Dassault Systemes, SIMULIA) free drainage can be achieved if $k_s \gg k_{vel}/\gamma_l c_{el}$, where $k_{vel} = k \cdot \gamma_l$ is the hydraulic conductivity of the material of the callus, γ_l is the specific weight of the liquid and c_{el} is the characteristic length of the element next to the drainage surface.

Table 2. Finite element numbers in the models.

Tissue	Large callus	Small callus
Cortical bone	83,080	83,080
Marrow	54,432	56,160
Callus	79,705	41,454

Since in this part of the study the simulation of full free drainage conditions is not intended, as the large seepage coefficient the limit value $k_s \approx k/c_{el}$ is assumed, whereas as k the approximate value of mature bone permeability is presumed, i.e. $k \approx 1 \cdot 10^{-13}$, which is the most permeable tissue arising during the callus stiffening. Thus, the large seepage coefficient is set to $k_s^{\text{large}} = 10^{-13}/c_{el}$. The medium and small seepage coefficient are set arbitrary to $k_s^{\text{medium}} = 0.1k_s^{\text{large}}$, $k_s^{\text{small}} = 0.01k_s^{\text{large}}$, respectively.

3. Results

At first the two opposite permeability conditions for both callus sizes are considered. In Figure 2 the bone tissue formation for fully impermeable and fully permeable condition in large and small callus is presented. The results are presented until no significant changes in bone formation is noticed.

The tissue phenotype is identified basing on the resultant elastic modulus achieved in the considered region of the callus (Isaksson et al. 2006; Ma et al. 2018), i.e. $E \in \langle 500, 1000)$, $E \in \langle 1000, 2000)$, $E >$ 2000 MPa for immature, intermediate and mature bone, respectively. The fully permeable conditions at the callus external boundary slows down slightly the stiffening of its external part in the first stage of healing. For the large callus it is clearly visible up to the 21th day and for the small callus up to the 56th day. From this moment, the external callus starts to be composed of the mature bone only and the healing progress is faster if permeable conditions are enforced. The stiffening ratio does not depend substantially on the permeability conditions in the case of the large callus, however, a remarkable inhibition of bone formation at the interface between the cortical shaft and the medullary canal is observed in the case of the small impermeable callus.

Figures 3 and 4 present the evolution of the octahedral shear strain (γ) and interstitial fluid velocity (v) in arbitrary chosen points (P1–P4) of large and small calluses for permeable and impermeable conditions. The number of days shown in Figures 3(a) and 4(a) corresponds to the day at which the strain in all the considered points reaches zero. In the contrary, the evolution of velocity changes (Figures 3(b) and 4(b)) is shown for the same periods as in Figure 2. The points match characteristic regions: P1 – the center of the internal part of the analyzed half of the callus, P2 – center of the analyzed half of bone inter-fragmentary gap, P3 –

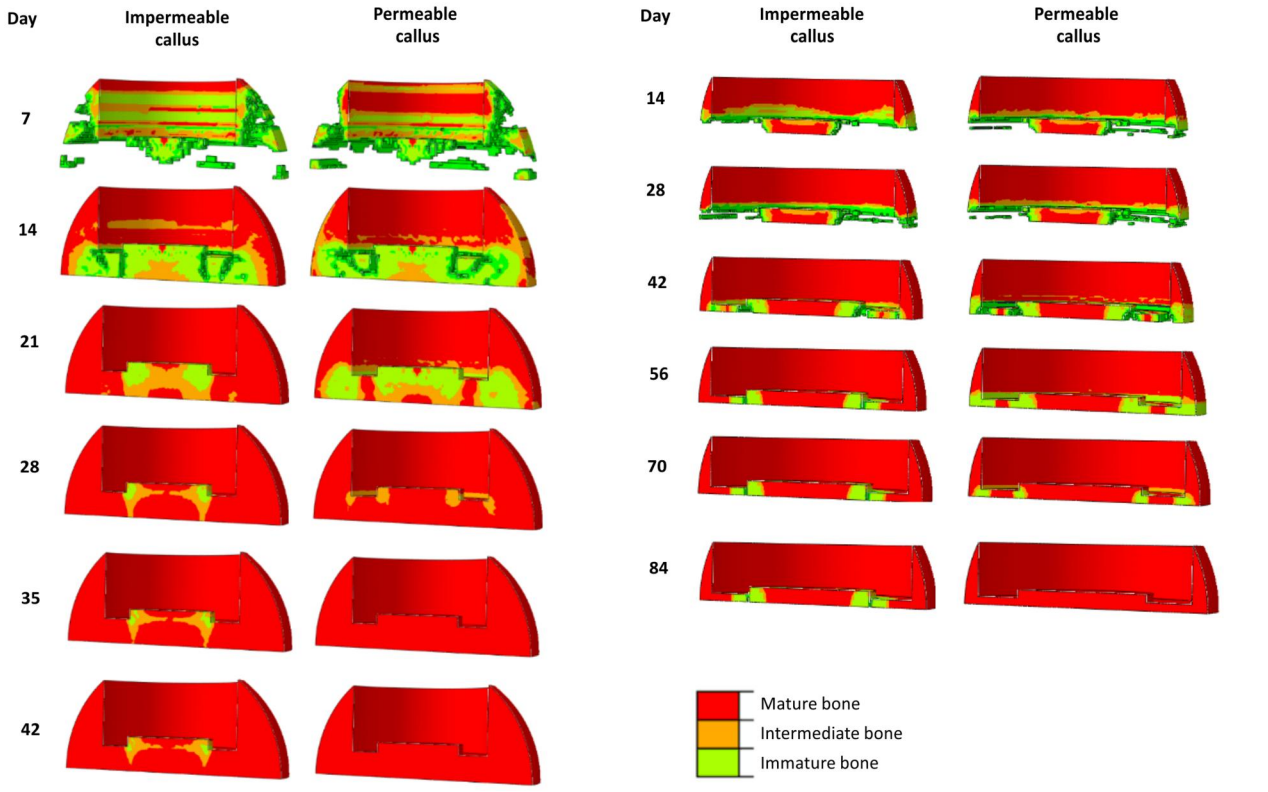

Figure 2. Comparison of bone tissue formation for permeable and impermeable conditions – large callus (left), small callus (right).

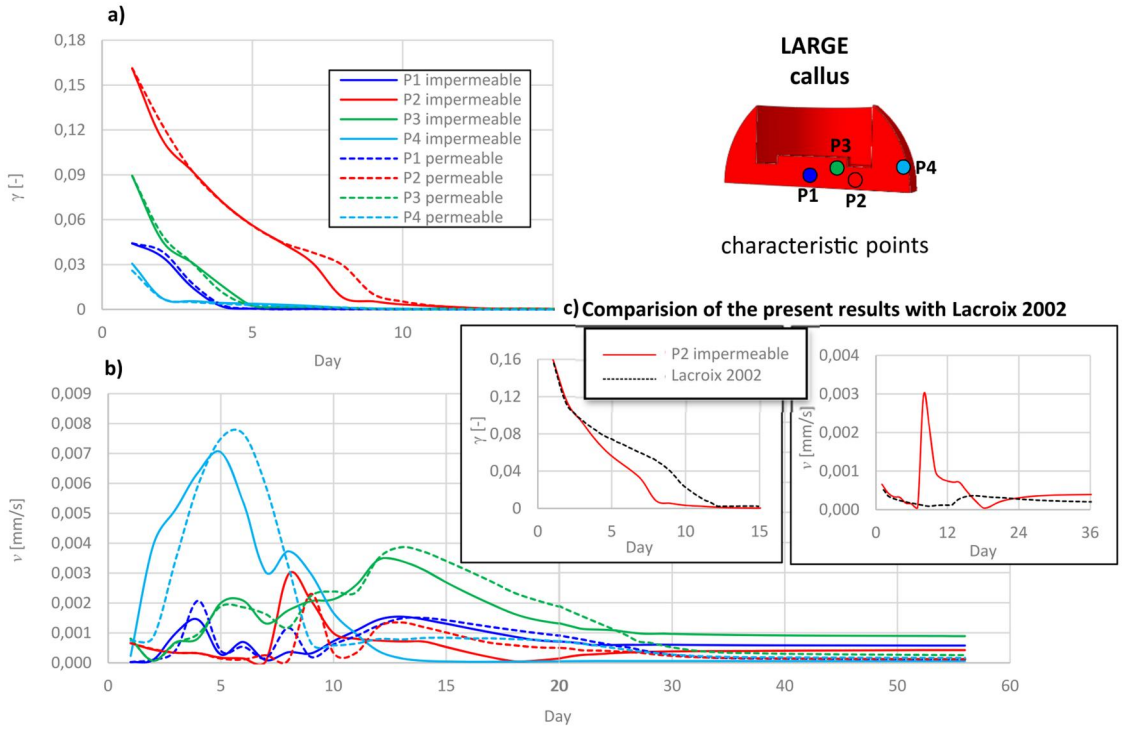

Figure 3. (a and b) Influence of permeability conditions on the octahedral shear strain (γ) and fluid velocity (v) in characteristic points of large callus. Comparison of the present model with (Lacroix et al. 2002).

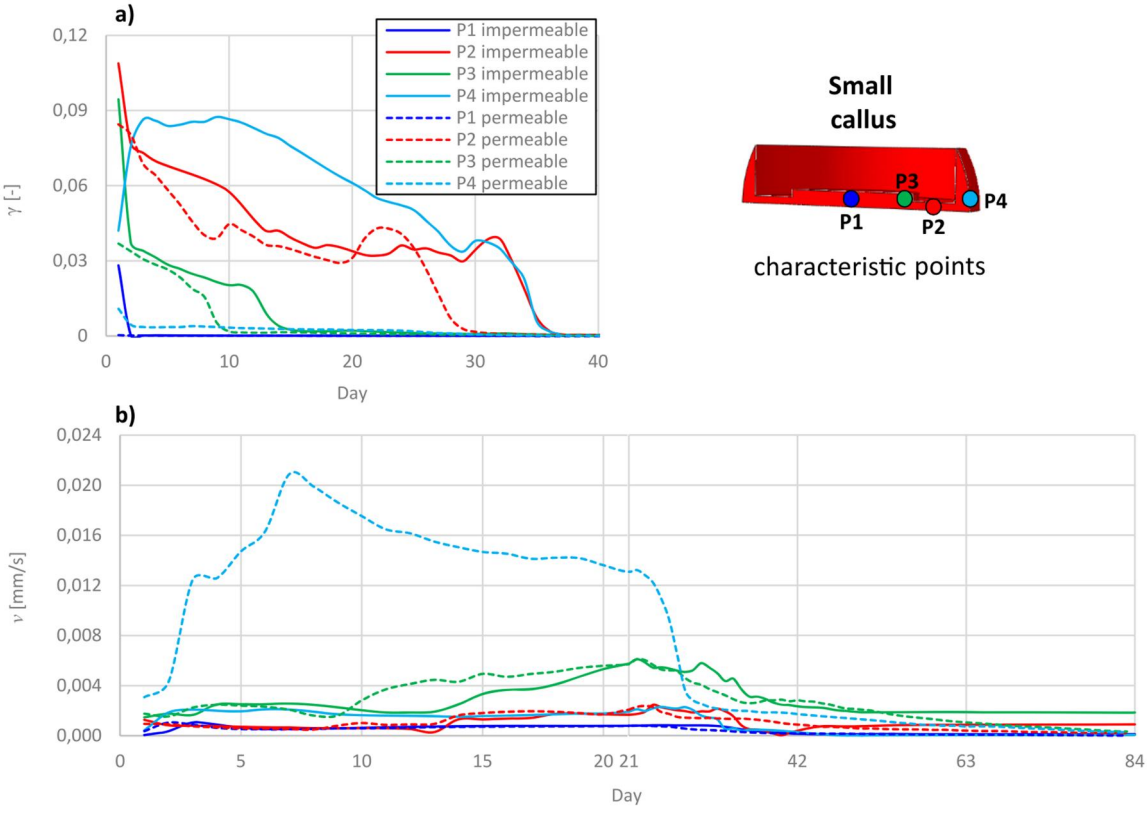

Figure 4. (a and b) Influence of permeability conditions on the octahedral shear strain (γ) and fluid velocity (v) in characteristic points of small callus.

region of the highest fluid velocities in the final stage of healing, P4 - external boundary of the gap. As for the case of the large impermeable callus a reference solution exists, additionally, in Figure 3 the comparison of the present results with curves reported in Lacroix et al. (2002) is shown. For this purpose the evolution of the strain and fluid velocity in point P2 is presented for the same time period as shown in Lacroix et al. (2002).

Independently of the callus size and the permeability conditions, the reduction of the deformability of the fracture site is caused by the formation of the external callus: it falls on ca. 12 d for large (Figure 3(a)) and on ca. 35 d for small (Figure 4(a)) callus, respectively, (cf. Figure 2).

Figure 3(a) shows clearly, that the permeability conditions do not influence essentially the mechanical flexibility of the large callus. They have an impact only on the velocity values (Figure 3(b)), which are slightly larger for the permeable conditions during the external callus formation and just after this phase. Thereafter they tends asymptotically to zero. The latter observation is not noticed for the impermeable callus. The impermeable conditions hinder the decrease of the velocity field in the internal callus (points P1, P2, P3, Figure 3(b)) – the velocity tends to zero very slowly. Though, the entire callus is filled with bone tissues after 3 weeks of simulation.

In the opposite, the callus permeability conditions start to play a more important role for smaller callus size. From Figure 4(a,b) it follows, that they influence substantially the velocity as well as the deformability of the external callus, especially in point P4. Impermeable conditions provide larger deformations of this region (Figure 4(a)) whereas full permeability enforces significantly larger fluid velocity (Figure 4(b)). Similarly as in the case of the large callus, the impermeability conditions hinder the reduction of the velocity values to zero in the cortical shaft (points P2, P3, Figure 4(b)), but in this case this leads to the inhibition of bone formation in this region.

For better understanding of the influence of the individual stimuli on the healing process, in Figures 5 and 6 the influence of permeability conditions on the biomechanical stimuli $S(\gamma) = \gamma/0.0375$ and $S(v) = v/0.003$ mm/s in characteristic points (P1-P4) of large and small callus is demonstrated. Figures 5(c,d) and 6(c,d) illustrate the evolution of the stimuli for the total period considered, cf. Figure 2, whereas Figures 5(a,b) and 6(a,b) illustrate shorter periods characterized by large fluctuations of stimuli.

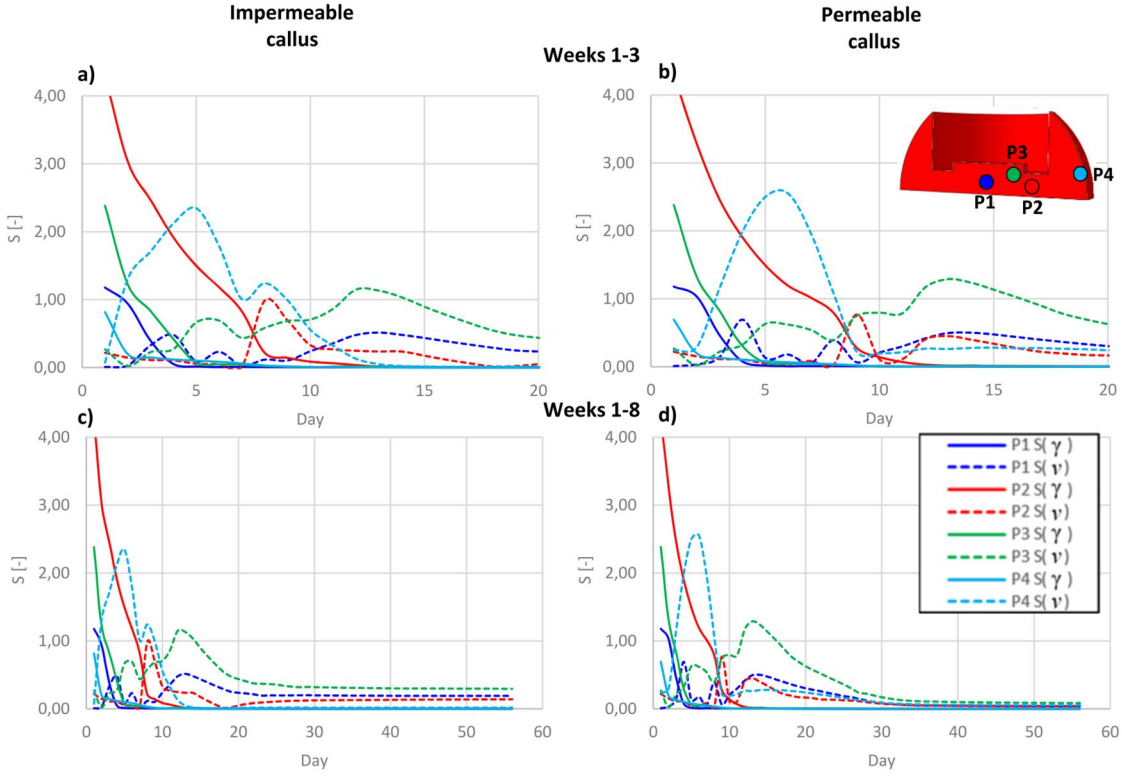

Figure 5. (a–d) Influence of permeability conditions on the biomechanical stimulus S(γ) and S(*v*) in characteristic points of large callus.

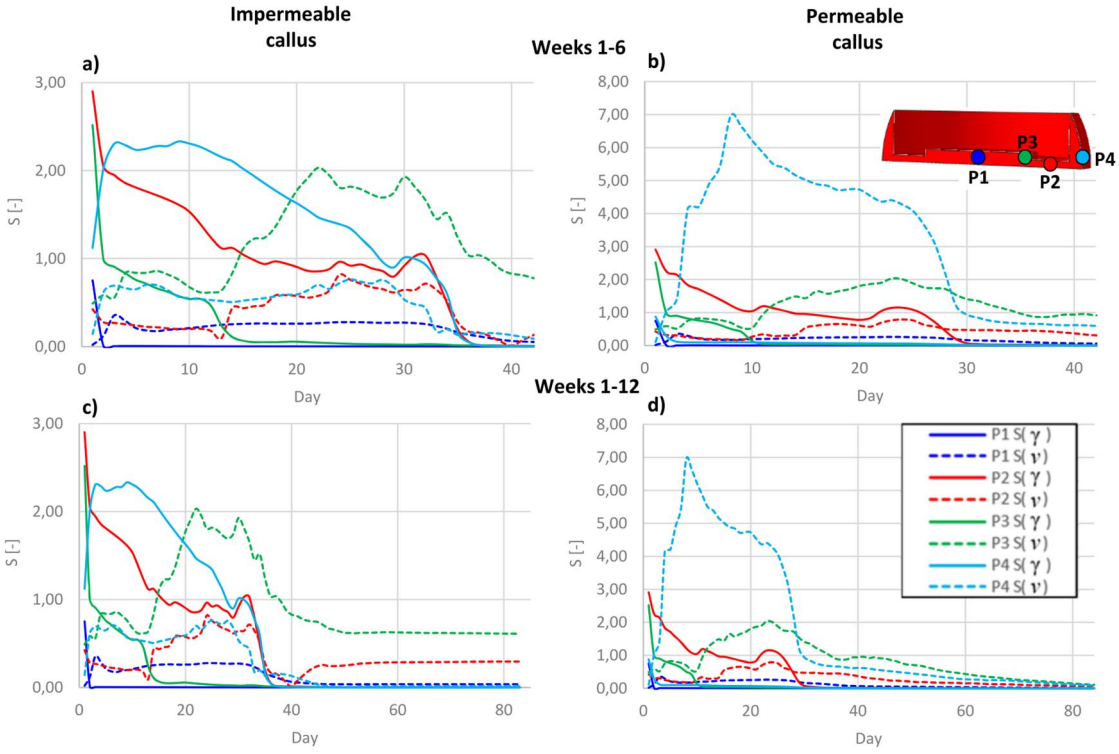

Figure 6. (a–d) Influence of permeability conditions on the biomechanical stimulus S(γ) and S(*v*) in characteristic points of small callus.

In large callus (Figure 5), independently on the permeability conditions, a characteristic interplay of both stimuli $S(\gamma) = \gamma/0.0375$ and $S(v) = v/0.003$ mm/s is observed. In all points studied, in the first stage, the deformation stimulus $S(\gamma)$ plays an essential role evidently. It decreases with the increase of the distance from the cortical shaft. The decrease of the deformation stimulus $S(\gamma)$, caused by the formation of the external callus, is followed by the increase of the velocity stimulus $S(v)$. The latter one after a certain number of days reduces asymptotically to zero or larger value, depending on the boundary permeability, cf. Figure 5(c,d).

Slightly different observations are made for the small callus (Figure 6). The deformation stimulus $S(\gamma)$ in the internal callus (points P1–P3) is comparable for both cases of permeability conditions, see Figure 6(a,b). Nonetheless, the callus impermeability provides essential deformation stimulus $S(\gamma)$ in the external callus (point P4), whereas the permeable boundary enforces large velocity stimulus $S(v)$ in this region, see Figure 6(a,b). These both stimuli remain high over 4–5 weeks and inhibit the formation of the external callus, cf. Figure 2. After this period the healing is governed by the velocity stimulus which decrease is reliant on the boundary permeability, see Figure 6(c,d).

While both, the fully impermeable and fully permeable boundary conditions, are rather not realistic, additional analyses were performed with intermediate drainage conditions. Since, as described above, the permeability conditions are pronounced only for the small size of the callus, only this case is considered more extensively.

Figure 7 depicts the comparison of the bone formation process in small callus with respect to different drainage conditions. Additionally, the pore pressure distribution for the last simulated day is shown. It must be stressed, that irrespective the assumed drainage conditions, pore pressure distribution remains qualitatively the same after the stiffening of the external callus. It can be seen, that the external permeability of the callus has an essential impact on the pore pressure distribution and flow direction at the fracture site. With the decrease of the boundary permeability the external pressure values and the overall pressure gradients in the callus increase. With the decrease of the seepage, the flow tends to be localized and oriented toward the medullary canal. Therefore, an increase of the fluid velocity at the interface between the cortical shaft and the marrow cavity is observed. For this reason the bone formation in this area is inhibited for fully impermeable conditions.

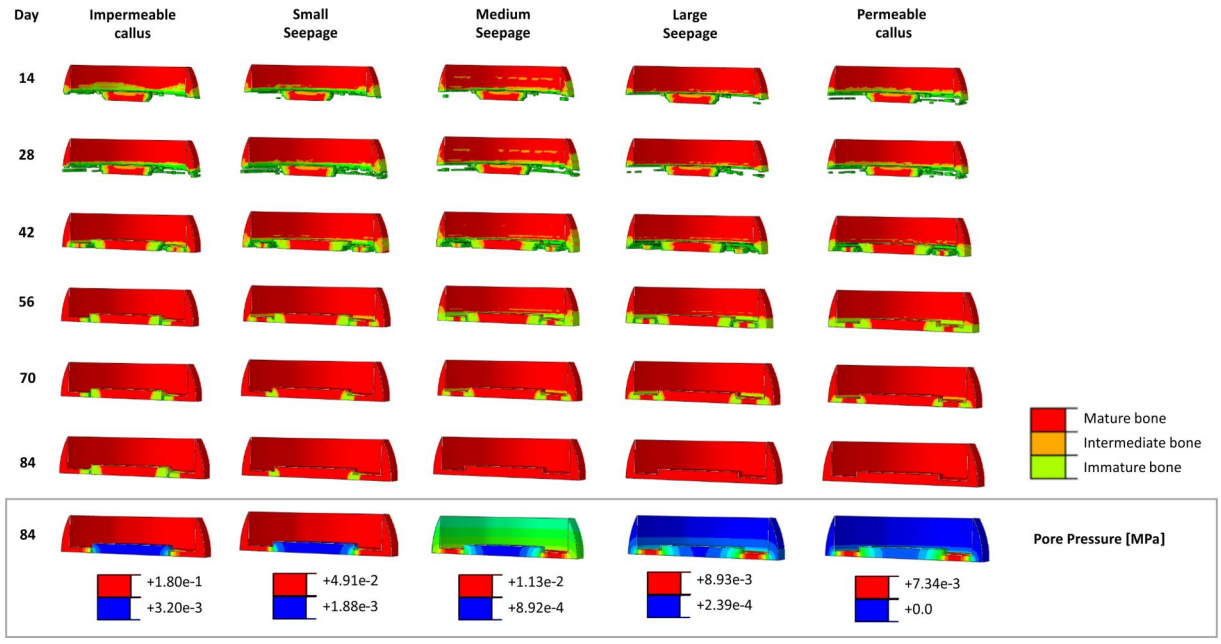

Figure 7. Influence of permeability conditions of the small callus on the bone tissue transformation in selected days and pore pressure distribution (day 84 only).

4. Discussion

4.1. Model verification

At first a comment on model verification shown in Figure 3(c) should be provided. It can be seen, that the present strain curve is in acceptable agreement with the reference solution (Lacroix et al. 2002). In the author's opinion the discrepancies can follow from various reasons, like other FEM program and other element formulation used in Lacroix et al. (2002), a different value of established diffusion coefficient, but especially from different smoothing strategy utilized in the update of material parameters. Additional tests performed by the author, assuming that the 10-days average is obtained even for the iterations less than 10, provide the delay of the callus stiffening and the resultant curve matches better the solution of Lacroix. Unfortunately, the smoothing strategy is not described in Lacroix et al. (2002).

On the other hand the discrepancy of the velocity curves is more pronounced. This can follow from the same factors, as mentioned above. It must be however stressed, that the velocity field becomes very irregular during the course of callus stiffening and the velocity curves fluctuate significantly over time, see (Lacroix et al. 2002). In the present study at around day 8 substantial velocity gradients arise in the vicinity of point P2. Thus, the quality of the curve is strongly dependent on the chosen point. Unfortunately, in Lacroix et al. (2002) the precise coordinates of the considered points are not provided. Thus, there is no guarantee that the same points are compared. Another reason that can cause these differences are the flow conditions at the interfaces of different tissues. In Abaqus by default the pore pressure consistency is imposed. It is not clear what kind of flow conditions are enforced in simulations in Lacroix et al. (2002) where a different FEM code, Diana, is employed. In the author's opinion different flow conditions at tissue interfaces can be also responsible for differences of the velocity field in the callus. Unfortunately, the velocity curve in Lacroix et al. (2002) is not provided for a longer period than ca. 36 days and it is difficult to decide, whether it tends to zero or not in further iterations.

Nonetheless, the stiffness distribution presented in Lacroix et al. (2002) indicates that after 20 d the callus is filled with bone tissues which is consistent with the present study, see Figure 2 (large impermeable callus). Thus, the overall healing pattern obtained in the present study matches the reference one, which proves the correct implementation of the model.

4.2. Influence of external permeability and size of the callus on simulation of bone healing progress

From the presented results it follows, that the larger callus heals faster. It should be noticed, that the geometry of the large callus was taken after (Lacroix et al. 2002). The fracture gap size (10 mm) assumed in there is pure theoretical. In fact, it is doubtful that gap of such size would heal in reality (Claes et al. 1997). Typical distance

between the bone fragments providing bone union achieve 1–3 mm (Lacroix and Prendergast 2002; Epari et al. 2006; Butler et al. 2007; Wehner et al. 2010; Miramini et al. 2016). The reason of the rapid healing of the large callus follows from the significant distance of the callus boundary from the cortical shaft which distributes the load to the fracture site. In consequence the MSC cells, which enter the callus from surrounding tissues are subjected to low biomechanical stimulus, cf. P4 in Figure 5. Thus, this zone stiffens very fast, leading in turn to the decrease of the octahedral strain, in the entire callus. In fact, it is questionable, that callus of such diameter ($d_{callus}/d_{bone} = 1.6$) can form in practice. Although such large d_{callus}/d_{bone} ratios assumed in the simulations of bone healing can be found in the literature (Wang and Yang 2018; Quinn et al. 2022b) rather lower values are most often reported, e.g. 1.4 (Isaksson et al. 2006; Byrne et al. 2011), 1.3 (Ma et al. 2018), 1.1 (Miramini et al. 2015; Miramini et al. 2016). In practice, the callus mass depends on the stabilization technique and other biological factors. Nonetheless, such large size seems unrealistic. In the present paper these dimensions were adopted for comparison purposes only, basing on the data provided in the pioneering work of Lacroix (Lacroix et al. 2002).

Although some numerical methods of prediction of the callus size can be also found in the literature (Comiskey et al. 2013; Mehboob and Chang 2018), in the present work the experimental investigations reported in Horn et al. (2011) were taken as a premise of the small callus' diameter. According to Horn et al. (2011) the ratio d_{callus}/d_{bone} is approximately 1.1. The gap dimension 2 mm assumed in the small callus is also more realistic.

In simulation the callus of such a size heals longer, since the MSC cells in its external part, cf. P4 in Figure 6, have unfavorable conditions for transformation into the hard phenotypes. Thus, the formation of the external callus which stabilizes the entire fracture site progresses slowly. What is more, at the final stage of healing, when the fluid flow play a crucial role, the fully impermeable conditions provide unfavorable pressure gradients within the callus leading to the increase of the fluid velocity in the region of the cortical shaft. This inhibits the healing progress in this zone.

4.3. Relevance of the study

The aim of the study is to evaluate influence of external permeability of the callus on simulation of bone healing progress. To the best of the author's knowledge the callus external boundary is usually assumed as impermeable in the simulations, see e.g. (Lacroix et al. 2002; Isaksson et al. 2006; Butler et al. 2007; Ma et al. 2018) and others. This assumption is frequently made without further explanation. The extended comment on this can be found e.g. in Isaksson et al. (2006). This condition is supposed to be provided by the fascia surrounding the fracture site.

Obviously, it is questionable if such tissue is present initially. It rather forms during the course of healing. However, since according to the present results, the permeability conditions do not affect the first phase of the process substantially, the lack of fascia in the first days does not need to be considered more extensively. The question is however, if it is fully impermeable, as it is most often assumed, and in what extent this full impermeability influences the results. In (Isaksson et al. 2006) it is stated, that callus permeability conditions have a minor effect on the tissues transformation in the fracture site. Though, the study was performed for relative large callus ($d_{callus}/d_{bone} = 1.4$). Present results confirm, that the fascia permeability does not have an significant impact on the healing process of large calluses. Nonetheless, its influence starts to be pronounced for smaller callus' diameters. Full impermeability of the callus boundary increases the pore pressure gradients and promotes the fluid flow towards the medullary canal. Due to the large gradients at the interface between the cortical shaft and the marrow canal, the fluid velocity is too large for the bone formation in this region. As shown, an assumed small drainage of the callus boundary reduces this adverse effect without essential qualitative changes of the pore pressure distribution in the entire callus. It provides the gap's closing after ca. 8 weeks (Figure 7), whereas the full impermeability inhibits this process and the union is not observed even after 12 weeks.

Although the size of the nonunion zone caused by the fully impermeable boundary is not considerable, in the author's opinion it is worth noticing, that in the simulations of healing of small callus the permeability of its boundary can be crucial after the maturation of its external parts. If such deceleration of the healing progress, as it is shown in the present study, is observed during the simulation, changing of the drainage conditions of the callus boundary can be a good remedy. It should not be treated as a numerical trick only, since in practice full impermeable boundary is only an assumption.

The model used in the present study possesses several limitations, as simplified geometry of the bone and callus, idealized loading conditions, etc. Moreover, the theoretical background of the bone healing simulation is not new. The model does not account for cells proliferation, blood vessel development and many other biological aspects. Some of these factors are included in newer studies e.g. (Byrne et al. 2011; Irandoust and Müftü 2020; Quinn et al. 2022b). These simplifications can be found as an essential restraint of the present study. However, in the author's opinion the conclusions drawn in this paper will be also valid for the enhanced simulations. Moreover, it is worth to stress, that the approach in such a basic form, as in the present analysis, is still widely used without any improvements, see e.g. (Chou and Müftü 2013; Ma et al. 2018; Mehboob et al. 2020) and others. Thus, the outcome of the paper is relevant.

As the study is only numerical, no hard clinical recommendations can be made. However, as the results show that the external permeability influences the healing process, it is worth to consider examination of this effect in experimental way. To the best of the author's knowledge the clinical studies focus usually on the stiffness of the fixators. Perhaps, flow and permeability conditions at the fracture site are also worthy attention.

4. Conclusions

In the paper the influence of the external permeability of the fracture callus on the simulation of the bone healing process is studied. Following conclusions can be drawn:

- Significance of the external permeability increases with the decrease of the callus size.
- Independent of the callus size full impermeable conditions improve the formation of the mature external callus. However, the effect is more pronounced for small callus.
- After the formation of a mature external callus full impermeable conditions slow down the healing progress. In small callus they provide unfavorable pressure gradients which inhibit the bone formation at the final stage of healing in the region of the cortical shaft.
- Independently of the callus size, the concept of the impermeable callus boundary in simulation is a 'safe' approach, since it provides finally worse conditions for healing. Thus, it can be always justified.
- Nonetheless, whenever a characteristic inhibition of the healing progress is observed in the simulation due to the deceleration of the velocities decrease, it is recommended to impose drainage conditions at the callus' boundary. Even small values of seepage can reduce the pore pressure gradients substantially and provide the reduction of velocity. Additional studies prove, that this conclusion is valid also for other bone and callus geometries and load directions.
- The drainage conditions of the callus' boundary are physically valid. Although the value of the seepage coefficient is unknown, a parametric study can be always performed to establish this quantity. It is reasonable to use such values which do not change the quality of the pore pressure distribution within the callus.

Acknowledgments

The calculations were carried out at the Academic Computer Centre in Gdansk, Gdansk University of Technology in Poland.

CRediT authorship contribution statement

Agnieszka Sabik: Conceptualization, Methodology, Software, Formal analysis, Visualisation, Writing – Original Draft.

Disclosure statement

The authors declare that they have no known competing financial interests or personal relationships that could have appeared to influenced he work reported in this paper.

Funding

The author(s) reported there is no funding associated with the work featured in this article.

Data availability statement

Data available on request from the authors.

References

Abaqus. 2021. Dassault Systems, SIMULIA.

Augat P, Faschingbauer M, Seide K, Tobita K, Callary SA, Solomon LB, Holstein JH. 2014. Biomechanical methods for the assessment of fracture repair. Injury. 45(Suppl 2): S32–S38. doi: 10.1016/j.injury.2014.04.006.

Augat P, Hollensteiner M, von Rüden C. 2021. The role of mechanical stimulation in the enhancement of bone healing. Injury. 52(Suppl 2):S78–S83. doi: 10.1016/j.injury.2020.10.009.

Beirami S, Nikkhoo M, Hassani K, Karimi A. 2021. A comparative finite element simulation of locking compression plate materials for tibial fracture treatment. Comput Methods Biomech Biomed Engin. 24(10):1064–1072. doi: 10.1080/10255842.2020.1867114.

Boccaccio A, Ballini A, Pappalettere C, Tullo D, Cantore S, Desiate A. 2011. Finite element method (FEM), mechanobiology and biomimetic scaffolds in bone tissue engineering. Int J Biol Sci. 7(1):112–132. doi: 10.7150/ijbs.7.112.

Butler RJ, Marchesi S, Royer T, Davis IS. 2007. The effect of a subject-specific amount of lateral wedge on knee. J Orthop Res Sept. 25:1121–1127. doi: 10.1002/jor.

Byrne DP, Lacroix D, Prendergast PJ. 2011. Simulation of fracture healing in the tibia: mechanoregulation of cell activity using a lattice modeling approach. J Orthop Res. 29(10):1496–1503. doi: 10.1002/jor.21362.

Chou HY, Müftü S. 2013. Simulation of peri-implant bone healing due to immediate loading in dental implant treatments. J Biomech. 46(5):871–878. doi: 10.1016/j.jbiomech.2012.12.023.

Claes L, Augat P, Suger G, Wilke HJ. 1997. Influence of size and stability of the osteotomy gap on the success of fracture healing. J Orthop Res. 15(4):577–584. doi: 10.1002/jor.1100150414.

Claes L. 2011. Biomechanical principles and mechanobiologic aspects of flexible and locked plating. J Orthop Trauma. 25(Suppl 1):S4–S7. doi: 10.1097/BOT.0b013e318207093e.

Comiskey D, MacDonald BJ, McCartney WT, Synnott K, O'Byrne J. 2013. Predicting the external formation of callus tissues in oblique bone fractures: idealised and clinical case studies. Biomech Model Mechanobiol. 12(6):1277–1282. doi: 10.1007/s10237-012-0468-6.

Epari DR, Taylor WR, Heller MO, Duda GN. 2006. Mechanical conditions in the initial phase of bone healing. Clin Biomech. 21(6):646–655. doi: 10.1016/j.clinbiomech.2006.01.003.

Feng YJ, Lin KP, Tsai CL, Wei HW. 2021. Influence of gap distance between bone and plate on structural stiffness and parallel interfragmental movement in far-cortical locking technique - a biomechanical study. Comput Methods Biomech Biomed Engin. 24(11):1206–1211. doi: 10.1080/10255842.2020.1870964.

Foster AL, Moriarty TF, Zalavras C, Morgenstern M, Jaiprakash A, Crawford R, Burch MA, Boot W, Tetsworth K, Miclau T, et al. 2021. The influence of biomechanical stability on bone healing and fracture-related infection: the legacy of Stephan Perren. Injury. 52(1):43–52. doi: 10.1016/j.injury.2020.06.044.

Horn C, Döbele S, Vester H, Schäffler A, Lucke M, Stöckle U. 2011. Combination of interfragmentary screws and locking plates in distal meta-diaphyseal fractures of the tibia: a retrospective, single-centre pilot study. Injury. 42(10):1031–1037. doi: 10.1016/j.injury.2011.05.010.

Huiskes R, Van Driel WD, Prendergast PJ, Søballe K. 1997. A biomechanical regulatory model for periprosthetic fibrous-tissue differentiation. J Mater Sci Mater Med. 8(12):785–788. doi: 10.1023/A:1018520914512.

Irandoust S, Müftü S. 2020. The interplay between bone healing and remodeling around dental implants. Sci Rep. 10(1):4335. doi: 10.1038/s41598-020-60735-7.

Isaksson H, van Donkelaar CC, Ito K. 2009. Sensitivity of tissue differentiation and bone healing predictions to tissue properties. J Biomech. 42(5):555–564. doi: 10.1016/j.jbiomech.2009.01.001.

Isaksson H, Wilson W, van Donkelaar CC, Huiskes R, Ito K. 2006. Comparison of biophysical stimuli for mechano-regulation of tissue differentiation during fracture healing. J Biomech. 39(8):1507–1516. doi: 10.1016/j.jbiomech.2005.01.037.

Lacroix D, Prendergast PJ, Li G, Marsh D. 2002. Biomechanical model to simulate tissue differentiation and bone regeneration: application to fracture healing. Med Biol Eng Comput. 40(1):14–21. doi: 10.1007/BF02347690.

Lacroix D, Prendergast PJ. 2002. A mechano-regulation model for tissue differentiation during fracture healing: analysis of gap size and loading. J Biomech. 35(9):1163–1171. doi: 10.1016/S0021-9290(02)00086-6.

Ma S, Zhou B, Markert B. 2018. Numerical simulation of the tissue differentiation and corrosion process of biodegradable magnesium implants during bone fracture healing. Z Angew Math Mech. 98(12):2223–2238. doi: 10.1002/zamm.201700314.

Mehboob A, Chang SH. 2018. Effect of composite bone plates on callus generation and healing of fractured tibia with different screw configurations. Compos Sci Technol. 167:96–105. doi: 10.1016/j.compscitech.2018.07.039.

Mehboob A, Chang SH. 2019. Effect of initial micro-movement of a fracture gap fastened by composite prosthesis on bone healing. Compos Struct. 226:111213. doi: 10.1016/j.compstruct.2019.111213.

Mehboob A, Mehboob H, Ouldyerou A, Barsoum I. 2024. Computational biomechanical analysis of Ti-6Al-4V porous bone plates for lower limb fractures. Mater Des. 240:112842. doi: 10.1016/j.matdes.2024.112842.

Mehboob A, Rizvi SHA, Chang SH, Mehboob H. 2020. Comparative study of healing fractured tibia assembled with various composite bone plates. Compos Sci Technol. 197:108248. doi: 10.1016/j.compscitech.2020.108248.

Merdji A, Taharou B, Hillstrom R, Benaissa A, Roy S, Chong PL, Mukdadi O, Della N, Bouiadjra BA. 2020. Finite-element study of biomechanical explanations for bone loss around dental implants. J Long Term Eff Med Implants. 30(1):21–30. doi: 10.1615/JLongTermEffMedImplants.2020035028.

Miramini S, Zhang L, Richardson M, Mendis P, Ebeling PR. 2016. Influence of fracture geometry on bone healing under locking plate fixations: a comparison between oblique and transverse tibial fractures. Med Eng Phys. 38(10):1100–1108. doi: 10.1016/j.medengphy.2016.07.007.

Miramini S, Zhang L, Richardson M, Pirpiris M, Mendis P, Oloyede K, Edwards G. 2015. Computational simulation of the early stage of bone healing under different configurations of locking compression plates. Comput Methods Biomech Biomed Eng. 18(8):900–913. doi: 10.1080/10255842.2013.855729.

Nayak GS, Roland M, Wiese B, Hort N, Diebels S. 2024. Influence of implant base material on secondary bone healing: an in silico study. Comput Methods Biomech Biomed Eng. 0(0):1–9. doi: 10.1080/10255842.2024.2338121.

Perren SM. 1979. Physical and biological aspects of fracture healing with special reference to internal fixation. Clin Orthop Relat Res. 138(138):175–196.

Prendergast PJ, Huiskes R, Søballe K. 1997. Biophysical stimuli on cells during tissue differentiation at implant interfaces. J Biomech. 30(6):539–548. doi: 10.1016/S0021-9290(96)00140-6.

Quinn C, Kopp A, Vaughan TJ. 2022a. A coupled computational framework for bone fracture healing and long-term remodelling: investigating the role of internal fixation on bone fractures. Int J Numer Method Biomed Eng. 38:e3609. doi: 10.1002/cnm.3609.

Quinn C, Kopp A, Vaughan TJ. 2022b. A coupled computational framework for bone fracture healing and long-term remodelling: investigating the role of internal fixation on bone fractures. Numer Methods Biomed Eng. 38(7):e3609. doi: 10.1002/cnm.3609.

Taharou B, Merdji A, Hillstrom R, Benaissa A, Roy S, Della N, Aid A, Mukdadi OM. 2021. Biomechanical evaluation of bone quality effect on stresses at bone-implant interface: a finite element study. J Appl Comput Mech. 7(3): 1266–1275. doi: 10.22055/jacm.2020.32323.2005.

Wang M, Yang N. 2018. Three-dimensional computational model simulating the fracture healing process with both biphasic poroelastic finite element analysis and fuzzy logic control. Sci Rep. 8(1):6744. doi: 10.1038/s41598-018-25229-7.

Wehner T, Claes L, Niemeyer F, Nolte D, Simon U. 2010. Influence of the fixation stability on the healing time—A numerical study of a patient-specific fracture healing process. Clin Biomech. 25(6):606–612. doi: 10.1016/j.clinbiomech.2010.03.003.